Mon. Not. R. Astron. Soc. **000**, 1–?? (2015) Printed 5 January 2016 (MN LATEX style file v2.2)

The dearth of nuclear star clusters in bright galaxies

M. Arca-Sedda[1⋆], R. Capuzzo-Dolcetta[1] and M. Spera[2]
[1] *Dept. of Physics, Sapienza, University of Rome, Piazzale Aldo Moro 5, I-00185, Rome (Italy)*
[2] *INAF - Osservatorio Astronomico di Padova, Vicolo dell' Osservatorio 5, I-35122 Padova, Italy*

arXiv:1510.01137v3 [astro-ph.GA] 4 Jan 2016

Revised to 09-2015

ABSTRACT

We investigate the interaction of a massive globular cluster (GC) with a super massive black hole (SMBH), located at the centre of its host galaxy, by means of direct N-body simulations. The results show that tidal distortions induced by the stellar background and the SMBH act on a time shorter than that of dynamical friction decay for a 10^6 $M_\odot$ GC whenever the SMBH mass exceeds $\sim 10^8$ $M_\odot$. This implies an almost complete dissolution of the infalling GC before it reaches the inner region ($\lesssim 5$ pc) of the parent galaxy. The generalization of this result to a larger sample of infalling GCs shows that such destructive process may prevent the formation and growth of a bright galactic nucleus. Another interesting, serendipitous, result we obtained is that the close interaction between the SMBH and the GC produces a "wave" of stars that escape from the cluster and, in a fraction, even from the whole galaxy.

Key words: galaxies: nuclei; galaxies: star clusters; methods: numerical.

1 INTRODUCTION

A galactic nucleus is a region where various astrophysical phenomena co-exist. Thanks to the high resolution images provided by the Hubble Space Telescope, it is clear, nowadays, that the nuclei of the majority of elliptical and early type spiral galaxies (with mass $\gtrsim 10^{10} M_\odot$) harbor massive and supermassive black holes (SMBHs) (Urry & Padovani 1995; Ferrarese & Ford 2005; Graham et al. 2011; Shankar et al. 2009; Kormendy & Ho 2013; Merritt 2013; Graham 2015). SMBHs have masses from $\sim 10^6$ $M_\odot$, up to the extreme case of the galaxy NGC1277, which hosts a SMBH with mass $\sim 1.7 \times 10^{10}$ $M_\odot$ (van den Bosch et al. 2012), although this mass estimation is very uncertain (Emsellem 2013).

In some cases, the SMBH is surrounded by a nuclear star cluster (NSC), a massive and dense stellar system composed of up to 10^8 stars (Carollo et al. 1997; Böker et al. 2002a; Côté et al. 2006; Wehner & Harris 2006; Graham & Driver 2007; Graham & Spitler 2009). In general, fainter galaxies host a NSC without evidence of the presence of a central massive black hole. Hence, it seems that there is a continuos sequence from NSC-dominated galaxies to SMBH-dominated galaxies (Bekki & Graham 2010). Due to this, SMBHs and NSCs are often indifferently referred to as compact massive objects (CMOs).

NSCs are observed in galaxies of any type in the Hubble sequence (Richstone et al. 1998; Carollo et al. 1997; Böker et al. 2002b; Côté et al. 2006; Turner et al. 2012; den Brok et al. 2014) and their channels of formation and evolution are still matter of debate. What we know, at present, is that NSCs are very massive ($10^6 - 10^7$ $M_\odot$) (Walcher et al. 2005), with a half-light radius of $2-5$ pc (Geha et al. 2002; Böker et al. 2004), and much more luminous ($\sim$4 mag) than ordinary galactic GCs.

Generally, NSCs contain both an old stellar population, age $\gtrsim 1$ Gyr, and a younger one, with ages below 100 Myr (Rossa et al. 2006). Furthermore, NSCs are located at the photometric and kinematic centre of their host galaxy, i.e. at the bottom of its potential well (Böker et al. 2002b; Neumayer et al. 2011).

Small sizes and large masses make NSCs the densest stellar systems observed in the Universe (Neumayer 2012).

Two are the most popular, and debated, formation scenarios:

- the one commonly referred to as "*in-situ model*", relies upon several injections of gas that accretes onto the central SMBH, leading to the formation and growth of a NSC (King 2003; Milosavljević 2004; King 2005; McLaughlin et al. 2006; Bekki 2007; Nayakshin et al. 2009; Hopkins & Quataert 2010; Antonini et al. 2015a);
- the scenario which is usually known as "*dry-merger scenario*". In this case, the main engine is the action of dynamical friction that causes the sink of massive GCs toward the galactic centre (Tremaine et al. 1975; Tremaine 1976; Capuzzo-Dolcetta 1993; Antonini 2013; Arca-Sedda & Capuzzo-Dolcetta 2014a). Decaying clusters merge in the central galactic region leading to the formation, and subsequent growth, of a NSC. This formation channel has been

⋆ E-mail: m.arcasedda@gmail.com

studied by several authors, through N-body simulations (Capuzzo-Dolcetta & Miocchi 2008a,b; Antonini et al. 2012; Arca-Sedda et al. 2015).

Currently, it is very difficult to discriminate between the two presented formation scenarios. However, the existence of scaling relations between the CMOs and their host galaxies may provide additional clues on the modes of growth and evolution of NSCs and SMBHs.

In particular Ferrarese et al. (2006) provided a power law relation between the NSC mass, $M_{\rm NSC}$, and the host velocity dispersion, σ, that is $M_{\rm NSC} \propto \sigma^4$. The in-situ model reproduces fairly well this correlation (Antonini 2013).

On the other hand, a more recent analysis based on larger datasets, provided a shallower power law relation, with exponent between 2 and 3 (Leigh et al. 2012; Erwin & Gadotti 2012; Graham 2012; Scott & Graham 2013); this shallower relation is in good agreement with the predictions of the dry-merger model (Antonini 2013; Arca-Sedda & Capuzzo-Dolcetta 2014b).

An interesting feature of NSCs is that they are very rare in galaxies with masses $\gtrsim 10^{11}{\rm M}_\odot$. These galaxies have luminosity profiles that do not show observational evidences of a central excess, which is widely considered a clear signature of the presence of a NSC (Côté et al. 2006; Turner et al. 2012; den Brok et al. 2014).

Various hypotheses have been raised to explain the observed absence of a nucleated region in massive galaxies. For instance, giant elliptical galaxies are thought to be the merging product of smaller galaxies. In this framework, if two colliding galaxies contain both a SMBH and a NSC, the central region of the merger product should borrow a SMBH binary, that may heat the surrounding nucleus, inducing its evaporation (Merritt 2006; Bekki & Graham 2010; Antonini et al. 2015b).

Another intriguing possibility is that the central SMBH prevents the NSC formation by tidally destroying its "building blocks", i.e. the decaying star clusters (Capuzzo-Dolcetta 1993; Antonini 2013; Arca-Sedda & Capuzzo-Dolcetta 2014b). As a consequence of the tidal stripping exerted on the decaying clusters, it is also possible that the newly born NSC is too small and, thus, very hard to detect through the analysis of the galactic luminosity profile.

On the other hand, as suggested recently by Arca-Sedda et al. (2015), the tidal action of a SMBH seems insufficient to quench the formation of NSCs in galaxies containing SMBHs with masses similar (or less than) that of the Milky Way.

Combining the scaling relations that link NSCs and SMBHs with their host galaxies, it is found that the SMBH mass threshold over which galaxies do not show any evidence for a nucleated region roughly corresponds to the condition $M_{\rm SMBH} \gtrsim M_{\rm NSC}$. As a matter of fact, no NSCs are observed in galaxies harboring very massive BHs at their centres; this could be the indication of a physical connection between the presence of NSCs and the SMBHs.

In this paper, we investigate the tidal action exerted by a SMBH and by the galactic region in which it moves, on an infalling GC, which is supposed to be one of the building blocks of a NSC.

The main aim of this research is understanding whether the tidal disruption process can inhibit the formation of a NSC or, at least, limit its mass (and luminosity) below an observationally detectable value.

To reach such a goal, we performed a set of direct N-body simulations of the inner region of a galaxy containing a central SMBH and an orbiting GC.

The paper is organized as follows: in Section 2 we present and discuss how we modelled the host galaxy and the GC, and the initial conditions selected for the simulations; our results are presented in Section 3 and discussed in Section 4. Finally, in Section 6, we draw the conclusions of this work.

2 MODELLING THE HOST GALAXY AND THE ORBITING CLUSTER

Using a series of high-precision, direct N-body simulations, we modelled the orbital decay of a single GC traversing the inner region of a galaxy containing a SMBH, whose mass is tightly correlated with the galaxy mass. We varied the SMBH and galaxy mass, in order to highlight how their tidal action influences the infall process of the GC.

In particular, we aim to shed light on which is the dominant process in shaping the inner region of galaxies: the dynamical friction, which drags GCs toward the galactic centre, making the formation of a NSC easier, or the tidal heating mechanism, which favours the disruption of the infalling GCs.

2.1 The host galaxy

A one-to-one N-body modelling of an entire galaxy requires an exceedingly large number of particles ($N \gtrsim 10^{11}$ for a typical galaxy). Nowadays, the state-of-the-art of direct N-body simulations limits such number to $N \sim 10^6$.

In order to keep the number of particles reasonably low without altering the correct behaviour of the system, avoiding spurious relaxation effects and ensuring a sufficient phase-space resolution, we restricted our model to a limited spatial region of the galaxy. To generate a dynamically stable model of the spatial region of interest, we adopted a truncated density profile, that, as suggested by McMillan & Dehnen (2007), has the form

$$\rho_{\rm tr}(r) = \frac{\rho(r)}{\cosh(r/r_{\rm tr})}, \tag{1}$$

where cosh is the hyperbolic cosine function, $r_{\rm tr}$ is the truncation distance, that we assume $r_{\rm tr} = 70$ pc, and $\rho(r)$ belongs to the class of the so-called (Dehnen 1993) profiles:

$$\rho(r) = \frac{(3-\gamma)M_g}{4\pi r_s^3}\frac{1}{(r/r_s)^\gamma(1+r/r_s)^{4-\gamma}}, \tag{2}$$

where M_g is the galaxy mass, r_s is its length scale and γ gives the inner slope of the density profile.

The density models considered in this paper have γ in the range $[0.2, 0.3]$. In particular, we selected γ in order to obtain a good compromise between the reliability of the galaxy model and the resolution of its N-body sampling.

Following this strategy, we used more than 1.5×10^4 particles to model the infalling GC, allowing a reliable description of its internal dynamics.

For the purposes of this work, we sampled 4 galaxy models with mass in the range $10^{10}\mathrm{M}_\odot < M_g < 3.2 \times 10^{11}\mathrm{M}_\odot$.

The mass of the SMBH hosted at the centre of the galaxy was set according to the scaling relation provided by Scott & Graham (2013):

$$\mathrm{Log}_{10}\left(\frac{M_{\rm BH}}{\mathrm{M}_\odot}\right) = \alpha \mathrm{Log}_{10}\left(\frac{M_g}{10^{11.3}\mathrm{M}_\odot}\right) + \beta, \qquad (3)$$

where $\alpha = 1.37 \pm 0.23$ and $\beta = 8.47 \pm 0.07$.

Table 1 summarises the main parameters that characterise our galactic representations.

2.2 The globular cluster model

The phase space distribution of the stars in the GC is generated according to the King distribution function (King 1966).

The mass of the GC model used in our simulation is $M = 10^6$ $\mathrm{M}_\odot$ since only such massive GCs have had time to sink toward the central galactic region, where we start our simulations.

The tidal radius, R_t, gives an estimate of the cluster size, and is evaluated with the relation (Binney & Tremaine 2008):

$$R_t^3 = \frac{GM}{\omega_p^2 + \left(\frac{\mathrm{d}^2\Phi}{dr^2}\right)_{r_p}}, \qquad (4)$$

where r_p is the perigalactic distance of the GC, ω_p is the angular velocity of the circular orbit of radius r_p, and $\Phi(r)$ is the galactic gravitational potential, assumed spherically symmetric.

Equation 4 is obtained assuming the cluster as a point of mass M. In our simulations, this hypothesis is acceptable because the typical core radius of the cluster (R_c) is much smaller than r_p, being $R_c/r_p \sim 0.03$.

The galactic potential, $\Phi(r)$, is given by the sum of the central BH potential and the smooth galactic background. Hence, the tidal force per unit mass acting on the GC at its pericentric distance is:

$$\left(\frac{\mathrm{d}^2\Phi}{dr^2}\right)_{r_p} = \frac{2GM_{\rm BH}}{r_p^3} - \frac{GM_g}{r_p^\gamma (r_p + r_s)^{4-\gamma}}\left[(1-\gamma)r_s - 2r_p\right]. \qquad (5)$$

The angular velocity ω_p in Equation 4 is:

$$\omega_p^2 = \frac{GM_{\rm BH}}{r_p^3} + \frac{GM_g}{r_p^3}\left(\frac{r_p}{r_p + r_s}\right)^{3-\gamma}. \qquad (6)$$

Equations 4, 5 and 6 make clear that the heavier the galaxy and the SMBH, the smaller the value of R_t at fixed values of the other parameters. In our simulations, the smaller value of R_t is achieved in the galaxy model characterised by $\mathrm{M_{BH}} = 5 \times 10^8$ $\mathrm{M}_\odot$ and $r_p \simeq 7$ pc, where $R_t \simeq 4$ pc.

The tidal radius of a GC modelled with a King profile is tightly connected to the adimensional potential well, W_0, and the core radius, R_c. To set these parameters, we ran a series of test simulations at varying W_0, R_c. We found that for $W_0 \lesssim 6$ and $R_c > 0.24$ pc, the GC is almost completely disrupted in less than a dynamical time, quite independently of the value of R_c. Hence, we choose for our GC model these two limiting values ($W_0 = 6$ and $R_c = 0.24$ pc), avoiding this way spurious tidal effects on the GC evolution.

In order to highlight the effects of the galactic nucleus and the SMBH on the orbital evolution of the GC, we decided to adopt the same GC model in all the simulations performed.

In our simulations, we followed the dynamical evolution of the GC, placed on circular, radial and eccentric orbits, starting at an initial distance $r_0 = 50$ pc from the central SMBH. We stopped our simulations when either the GC distance to the SMBH falls below 20 pc or the GC has lost 80% of its initial mass. With the choice of parameters given above, our GC models have 2-body relaxation times ($t_{\rm rel}$) exceeding tens of Myr in all the cases studied, thus implying evaporation times, $t_{\rm ev} \simeq 140 t_{\rm rel}$ (Binney & Tremaine 2008), much longer than the simulated time, which does not pass 130 Myr. We set the orbital parameters such that r_0 represents the initial apocentre in all the cases studied. This choice leads to orbits of different total energy, E_0, going from radial to circular orbits. However, the differences we found are smaller than 1%, as shown through the ratio $E_0/\Phi(r_{\rm tr})$, being $\Phi(r_{\rm tr})$ the potential energy evaluated at the truncation radius (see Table 2).

We choose such small orbits around the galactic centre because we want to study the effect of single or multiple close encounters between a massive GC and the central SMBH. From the computational point of view, the small orbital apocentres allow a good compromise between the numbers of particles used to model the GC and the galaxy, keeping a good level of resolution. It is worth noting that the BH influence radius encloses the GC orbit in the models with $M_{\rm g} > 10^{10}\mathrm{M}_\odot$.

Table 2 reports a synthetic outline of the orbital properties of our GC.

3 RESULTS

All our simulations have been run using `HiGPUs` (Capuzzo-Dolcetta et al. 2013), a highly parallel, direct summation, N-body code that fully exploits the computational power of Graphic Processing Units (GPUs).

The `HiGPUs` code implements a Hermite 6-th order integrator with block time steps and individual softening, ε, to smooth the gravitational interactions among the stars within the GC. In particular, we used $\varepsilon = 10^{-3}$ pc. This choice leads to a relative error on the mechanical energy in the range $10^{-6} - 5 \times 10^{-5}$ over the whole time extension of the simulations.

After several experiments, we found that a total number of particles $N \gtrsim 10^6$ was a good compromise between phase space resolution of the whole system (galaxy+SMBH+GC), and computing time, allowing us to carry out a wide set of simulations in a reasonable time. To study how the GC structure evolves as it moves around the galactic centre, we developed an analysis tool that provides, along the GC tra-

Table 1.

Parameters of the simulations

M_g ($10^{11}\mathrm{M}_\odot$)	$M_{\rm BH}$ ($10^8\mathrm{M}_\odot$)	r_s (pc)	$M_{\rm tr}$ ($10^7\mathrm{M}_\odot$)	σ (km/s)	$N_{\rm gal}$	m_* ($\mathrm{M}_\odot$)
0.1	5×10^-2	995	3.4	30	$1,018,742$	34
0.32	2×10^-1	1512	4.1	40	$1,024,025$	41
1.0	1	1917	5.9	70	$1,031,338$	57
3.2	5	2876	6.8	140	$1,033,332$	66

Col. 1: galaxy mass, Col. 2: BH mass. Col. 3: galaxy scale radius. Col. 4: galaxy mass within r_{tr}. Col. 5: velocity dispersion of the galaxy within 50 pc from the BH. Col. 6: number of particles used in the galaxy. Col. 7: individual particle mass.

Table 2.

GC orbital parameters

M_g ($10^{11}\mathrm{M}_\odot$)	r_p (pc)	e	$E_0/\Phi(r_{\rm tr})$	$v_0/v_c(r_0)$	N_{clu}
0.1	50	0	1.038	1	$29,832$
0.1	7.4	0.75	1.035	0.5	
0.1	0	1	1.025	0	
0.32	50	0	1.036	1	$24,550$
0.32	7.4	0.74	1.031	0.5	
0.32	0	1	1.017	0	
1.0	50	0	1.053	1	$17,237$
1.0	7.4	0.74	1.044	0.5	
1.0	0	1	1.018	0	
3.2	50	0	1.106	1	$15,243$
3.2	7.8	0.73	1.087	0.5	
3.2	0	1	1.106	0	

Col. 1: galaxy mass. Col. 2: pericentre of the orbit. Col. 3: eccentricity. Col. 4: ratio between the initial GC orbital energy and the potential energy at the truncation radius. Col. 5: ratio between the initial velocity of the cluster and the circular velocity at its initial position. Col. 6: number of particles used to model the GC.

jectory, estimates of the size and mass of the cluster. The determination of a centre for the GC is not a trivial task to accomplish, because the GC, during its motion, may be severely warped by the tidal forces. Hence, the simple use of the centre of mass (COM) can be unsatisfactory for an estimates of the GC mass, spatial size and determination of its position in the galaxy. This convinced us to develop a recursive, grid-based algorithm that allows a reliable determination of the GC centre of density (COD), which permits a better evaluation of its structural and orbital parameters.

Figure 1 shows the difference between the COM and the COD in the simulation with $M_g = 3.2\times10^{10}\mathrm{M}_\odot$; it is clear the importance in determing the actual centre of the cluster in a proper way.

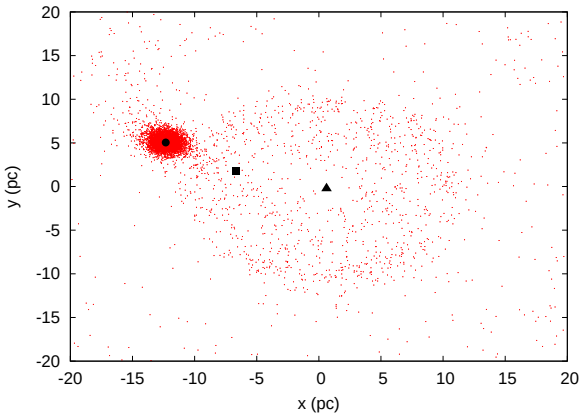

Figure 1. One snapshot of the simulation characterised by $M_g = 3.2\times10^{10}\mathrm{M}_\odot$. The red dots represent the stars in the GC, while the filled black triangle identifies the position of the BH. The filled black circle indicates the COD of the cluster, while the open black circle represents its COM.

3.1 Circular Orbits

The investigation of the effects of the interaction between the GC and the central SMBH has been done in the case of four different values of the galaxy mass, namely $M_g = 10^{10}, 3.2\times10^{10}, 10^{11}, 3.2\times10^{11}\mathrm{M}_\odot$, containing a SMBH, whose mass, obtained with Equation 3, is reported in Table 1.

In this Section, we discuss the results of the simulation of the evolution of a GC, placed on an initial circular orbit, at a distance $r_0 = 50$ pc from the galactic centre. The galactic centre in these cases coincides with the position of the SMBH, since we didn't found significant displacement of the SMBH during the evolution. Hence, in the following we assume that the galactic centre coincides with the position of the SMBH.

Figure 2 illustrates the GC distance from the SMBH, as a function of the time. It is evident that galaxies hosting lighter SMBHs allow the GC to reach an inner galactic region, whose size is comparable to the typical dimension

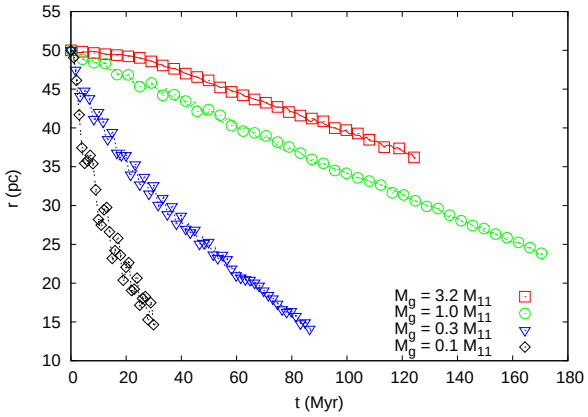

Figure 2. Time evolution of the GC distance to the BH in the four cases studied, as labelled in the plot.

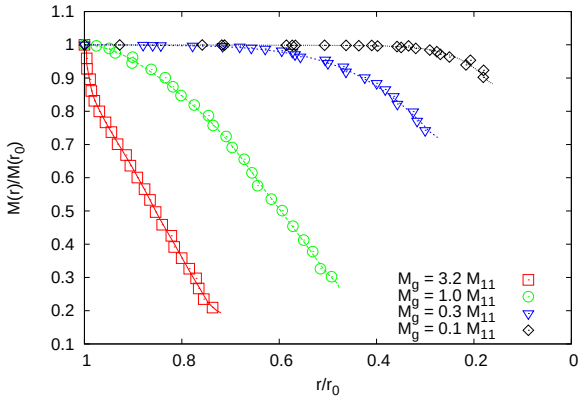

Figure 3. The ratio of the GC mass to its initial value as function of its distance to the central massive black hole, in the case of an initially circular GC orbit. Each curve refers to a galactic model as labelled.

of a NSC. On the other hand, heavier galaxies, harboring SMBHs more massive than $\sim 10^8 M_\odot$, efficiently shatter the GC, avoiding its decay to the innermost galactic region.

Figure 3 shows the mass of the GC, normalized to its initial value, as a function of the istantaneous distance of the GC from the SMBH. This plot, combined with Figure 2, allows to distinguish which mechanism dominates the GC evolution. Indeed, when tidal heating is the most effective phenomenon we should observe a rapid decrease of $M(r)/M(r_0)$ while r/r_0 decreases smoothly. On the other hand, if dynamical friction acts more efficiently than tidal heating, a nearly constant value of $M(r)/M(r_0)$ accompanies the r/r_0 decrease. The figure shows that tidal heating progressively deplete the GC of its stars for hosting galaxies more massive than 10^{11} $M_\odot$. On the other hand, the GC remains bound in lighter galaxies, and reach the inner region of the galaxy keeping more than 70% of its initial mass. Table 3 reports the radial distance of the GC from the galactic centre and the percentage of mass that remains bound to the GC at the end of our runs, making clear what stated above. The simulations ended at different times, since radial orbits decay faster than more roundish ones. Hence, the GC final mass listed in the table refers to different times.

Our results suggest that in a galaxy of mass above $\sim 10^{11}$ $M_\odot$ the combined bulge-SMBH tidal forces strip away from the GC most of its mass before it GC loses enough orbital energy to reach the inner galactic region. Conversely, below such *critical* value dynamical friction dominates over tidal heating, dragging the GC very close to the galactic centre.

3.2 Eccentric Orbits

Given the definition of orbital eccentricity as $e = (r_a - r_p)/(r_a + r_p)$, where r_a is the apocentric distance, after the circular ($e = 0$), we investigated also eccentric ($e > 0$) and radial ($e = 1$) orbits to understand how the orbital type influences the transport of matter toward the galactic centre influencing the process of formation of a stellar nucleus therein.

In the case of radial orbits, the cluster is placed at $r_0 = 50$ pc from the SMBH with zero initial velocity, while eccentric orbits are characterized by the GC starting at r_0 with an initial velocity $v = v_c(r_0)/2$, where $v_c(r_0)$ is the circular velocity at the galactocentric distance r_0. The direction of the initial velocity is orthogonal to the radius vector, leading to an eccentricity $e \simeq 0.7$.

Table 3.

GC final mass

M_g (10^{11}M$_\odot$)	$r_{\rm dec}$ (pc)	$M_{\rm dep}/M$ (%)
0.1	12	89
0.3	12	70
1.0	25	27
3.2	35	15

Column 1: mass of the host galaxy. Column 2: distance of the GC from the SMBH after the completion of the orbital decay process. Column 3: mass percentage which is still bound to the GC at the end of the simulation.

In these eccentric cases, the analysis of the GC structure is complicated in models with $M_g > 10^{11} M_\odot$, due to the difficulty to distinguish a clear centre and boundary for the GC after its first passage at pericentre.

Figures 4 and 5 show some snapshots of the GC orbital evolution for eccentric and radial orbits in the case $M_g = 3.2 \times 10^{11}$ $M_\odot$. In the case $e = 0.7$, it is worth noting that at every passage at pericentre some stars are stripped away from the GC and tend to move on precessing ellipses whose semi-major axes increase with the number of passages at pericentre. On the other hand, when the GC experiences an "head-on" collision with the SMBH, stars are scattered backward at different velocities, depending on the impact parameter that characterises each star-SMBH interaction. This peculiar interaction leads to the formation of a wake behind the former GC, with a structure similar to the propagation of a wave on a water plate.

Therefore, although it is quite difficult to identify the "core" of the GC, the interaction between an SMBH and an infalling GC produces debris that hides much informations about the initial orbital parameters of the GC.

However, due to the fact that it is almost impossible to identify a centre for the cluster in these cases, we limited our

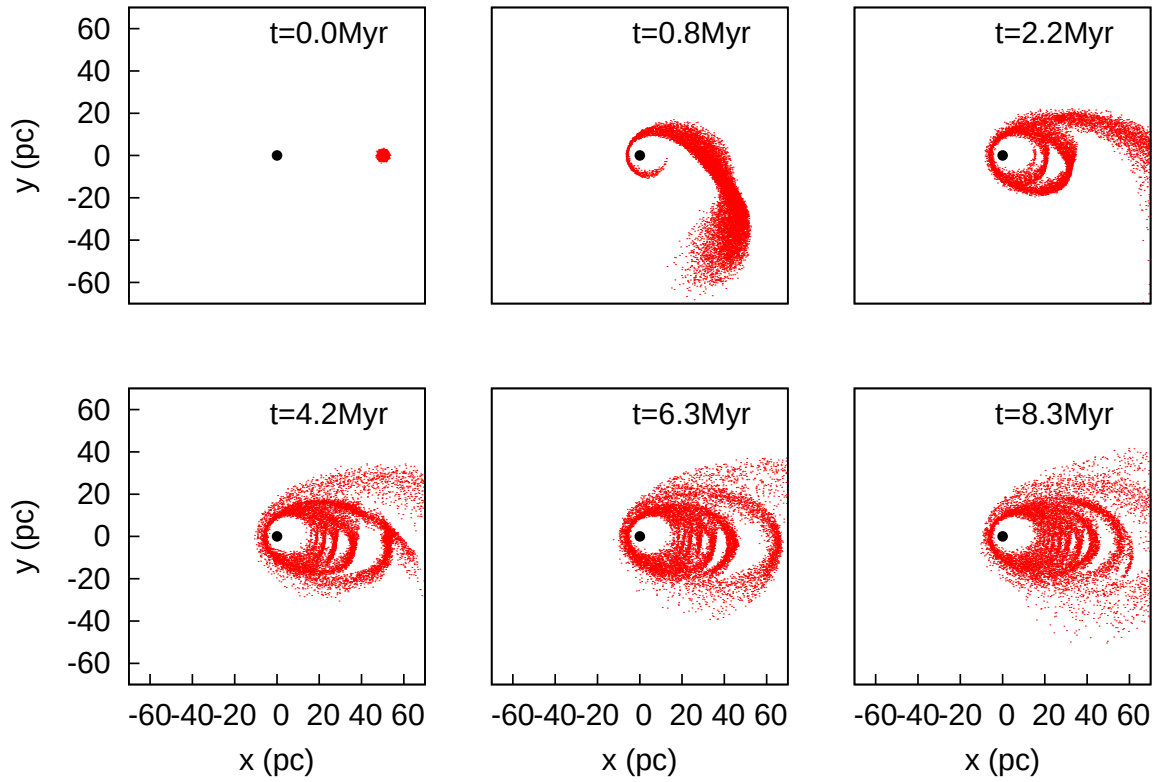

Figure 4. Snapshots at different times (labelled) of the cluster on an eccentric orbit in the case $M_g = 3.2 \times 10^{11} \mathrm{M}_\odot$. The central black dot represents the BH with mass $M_{\rm BH} = 5 \times 10^8 \mathrm{M}_\odot$. The x-y plane is the GC orbital plane.

analysis to the estimate of the amount of GC mass which remains confined to an inner region of the galaxy, around the SMBH.

When considering the simulations with $M_{\rm g} \geqslant 10^{11} \mathrm{M}_\odot$, we found that eccentric and radial orbits allow a more efficient transport of mass, toward the galactic centre, than circular orbits do. On these orbits, the GC can carry about 20% of its initial mass to the galactic centre, while, on circular orbits, such percentage is limited to few %. On the other hand, for lower galaxy masses, $M_{\rm g} < 10^{11} \mathrm{M}_\odot$, we found that the major contribution to the deposited mass comes from GC on circular orbits. We will deepen the discussion about these results in Section 4.

4 DISCUSSION

In this paper we have presented several N-body simulations to study the interaction between a single GC and a SMBH in the galactic centre. The results shed light on the actual mechanisms of mass accumulation in the central region of a massive galaxy ($M_g \geqslant 10^{11}$ $\mathrm{M}_\odot$).

Figure 6 shows the GC cumulative mass profile as a function of the distance from the SMBH after the orbital decay process, for all the orbits considered and in the case of $M_g = 10^{10} \mathrm{M}_\odot$ and $M_g = 3.2 \times 10^{10} \mathrm{M}_\odot$. Considering our lightest galaxy model, we found that circular and radial orbits are both efficient in the transport of mass toward the galactic centre. In such cases, the mass left to the galactic centre exceeds 80% of the initial mass of the GC. On the other hand, in heavier galaxy models, only GCs moving on initial nearly-radial orbits deposit a non negligible amount of their mass ($\sim$ 20% of the initial mass of the GC) in the inner 20 pc of the galaxy. Hence, the fraction of mass deposited within 20 pc from the SMBH varies from few percent, for the heaviest galaxy model, to more than 90% in the lightest.

We have shown that the mass deposition around the galactic centres is not efficient in galaxies with masses above $M_g = 10^{11} \mathrm{M}_\odot$. However, we cannot exclude that such (unefficient) mechanism may, eventually, drive the formation of a detectable, central overdensity. In order to address this point, we tried to reconstruct the projected, combined density profile of the host galaxy and its orbitally decayed GCs.

To do this, we consider a population of $N_{\rm GC}$ clusters whose orbits are evenly distributed among circular, eccentric ($e \simeq 0.7$) and radial.

Under the (extreme) assumption of "linearity" of the decay process, we can evaluate the global density profile as the mere sum of the density profile of the galaxy, $\rho_g(r)$, and of the decayed clusters:

$$\rho(r) = \rho_g(r) + \sum_{i=1}^{3} \alpha_i \rho_{e_i}(r), \qquad (7)$$

where α_i represent the fraction of GCs with initial eccentricity e_i. In the following calculations, we used $\alpha_i = 1/3$, and $e_1 = 0$, $e_2 = 0.7$, $e_3 = 1$.

It should be noted that the detectability of a nucleus

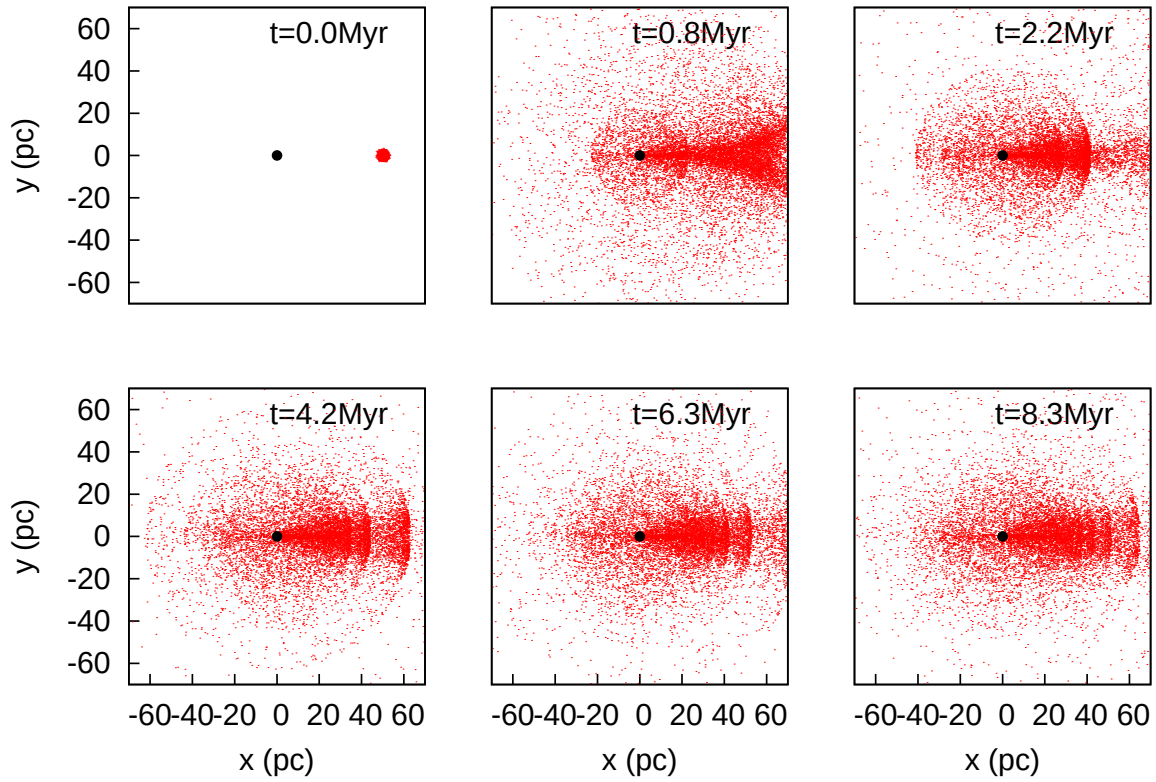

Figure 5. Same as in Figure 4, but for a cluster on a radial orbit.

through the analysis of the projected density profiles depends on the resolution of the instrument used to look at the target galaxy and the distance of the target itself. Due to this, in Figure 7 we assumed the host galaxy at the distance of the Virgo cluster (taken as 16.5 Mpc (Mei et al. 2007)), where a quite large number of NSCs have been detected over time Côté et al. (2004, 2006); Ferrarese et al. (2006).

Generally, the presence of a NSC in a galactic centre is argued by the presence of a clear edge in the projected inner luminosity profile of the host galaxy. Hence, a parameter that can be used to discriminate wheter or not a NSC resides in the centre of a galaxy is the surface density contrast $\delta\Sigma/\Sigma$ between the total (galaxy+GC) and the galactic background. We found that in our simulations the surface density contrast is related to the number of orbitally segregated clusters, $\delta\Sigma/\Sigma \propto N^k$, with $k \simeq 0.87$.

Galaxies with a clearly visible nucleated region have typical values $\delta\Sigma/\Sigma \sim 10$ (Côté et al. 2006; den Brok et al. 2014). On the base of our simulations we deduce that such values can be achieved only when more than 100 clusters with masses $\sim 10^6$ $M_\odot$ reach the galactic centre within a Hubble time.

Consequently, the missing evidence of NSCs in a galaxy of mass $M_g = 3.2 \times 10^{11} M_\odot$ would mean that in such galaxy there have not been enough GCs to merge and form it. This result agrees with previous findings by Arca-Sedda & Capuzzo-Dolcetta (2014b) indicating that in a galaxy with that mass the number of clusters which can decay and contribute to the formation of a nucleus is less than ~ 100.

Hence, the disruptive mechanism proposed here represents a satisfactory alternative to other theories, such as the disruption of pre-existing NSCs after a major merger event, or the tidal heating caused by a massive BH binary at the centre of the host galaxy. It is worth highlighting that our proposed mechanism requires only two ingredients, well supported by theoretical and observational arguments, that are: i) the presence of a SMBH within the galactic centre, and ii) the presence of a populations of star clusters around it. Moreover, it involves time-scales which are significantly shorter than those expected for galaxy merging and BHB formation.

5 HIGH VELOCITY STARS FROM GC-MBH ENCOUNTERS

The simulation of the interaction of the GC with the central massive galactic black hole showed an interesting side effect: after the fly-by around perigalacticon, a certain amount of stars are extracted from the GC and some of them even from the galaxy, on a privileged direction along the GC trajectory.

In the galaxy hosting the most massive BH, $M_{\rm BH} = 5 \times 10^8$ $M_\odot$, after the passage at perigalacticon, some stars in the GC gain velocities up to ~ 850 kms^{-1}. A fraction of them leave the galaxy reaching distances up to ~ 15 kpc in 60 Myr and (nearly constant) residual velocities up to ~ 250 kms^{-1}.

We performed a careful investigation to check whether

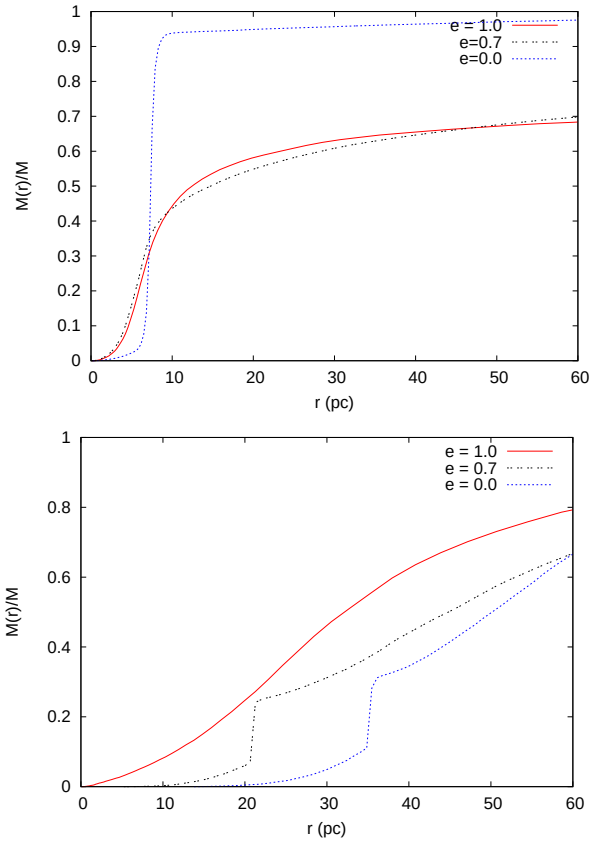

Figure 6. Cumulative mass profile of the GC, normalised to its initial mass, at the end of the simulations. The galaxy models considered here are $M_g = 10^{10}$ M$_\odot$ (top panel), and $M_g = 3.2 \times 10^{11}$ M$_\odot$ (bottom panel). In each panel, the various lines refer to GC orbits of the intial eccentricity labeled on top.

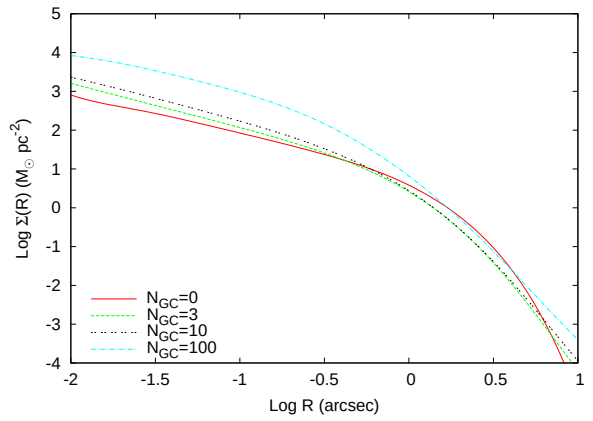

Figure 7. Projected density profile of the galaxy (red line) compared to the density profile in the cases of full decay of different numbers of GCs ($N_{\rm GC}$) as labelled.

it was a real effect or due to errors related to the numerical integration. This was done comparing the simulation results with those coming from extremely accurate integrations (although with a reduced number of particles) performed using a serial, fully regularized version of our N-body code, where regularization is applied to the whole set of pair interactions.

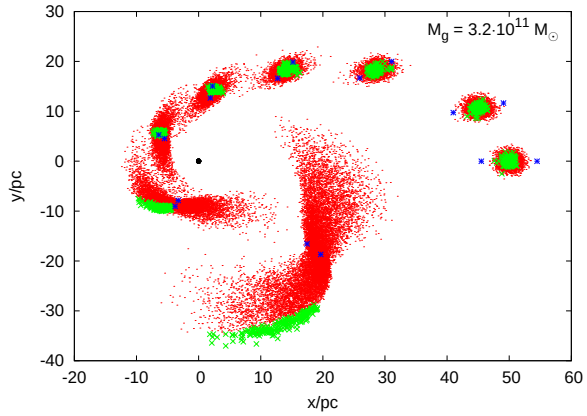

Figure 8. Various snapshots of the GC moving in a counter clockwise motion on an eccentric orbit. Escaping stars are green crosses, while red dots identify the stars that remain bound to the cluster. The black filled circle labels the SMBH, while the blue asterisks represent the lagrangian points L1 and L2. After the passage at pericentre, stars are thrown through L2.

Its use allowed us to keep the variation of the total mechanical energy of the system below 10^{-13}. This code employs the Mikkola's algorithmic regularization (Mikkola & Tanikawa 1999; Preto & Tremaine 1999), coupled with the chain algorithm, in order to handle efficiently very large particle mass ratios, like those we have in this work (massive black hole respect to the star mass). Results of this code (applied to a subsample of objects) confirmed that the effect was real and not a numerical artifact. Actually, we simulated the orbital evolution of the GC in the case $M_{\rm BH} = 5 \times 10^8$ M$_\odot$. Since our fully regularized, serial, N-body is hugely time consuming, we simulated only the first passage at the pericentre of our GC, sampled with ~ 50 particles. We found that the fraction of stars that leave the cluster and their velocities agree very well with the values obtained in the "extended" case.

It is worth noting that the escape velocity from the whole system, evaluated in our most massive model at perigalacticon, is, in our most massive model, $v_e(r_p) \leqslant 771$ kms^{-1}, while the escape velocity from the cluster is ~ 90 kms^{-1}. Hence, a fraction of the total number of stars are possible candidate as escapers, i.e. as stars energetically unbound from the galaxy and the GC.

In Figure 8 we present some snapshots of the GC moving in the $M_g = 3.2 \times 10^{11}$M$_\odot$ galaxy on the $e \simeq 0.7$ orbit, through its first perigalacticon passage, marking in color the escaping stars. After the passage at the pericentre, stars flow away through the lagrangian point L2, along the direction tangential to the GC trajectory. Therefore, the ejection occurs on a preferential direction, leading the escapers to move in a sort of "collimated beam".

We identified as escapers from the galaxy those stars that both i) get a positive mechanical energy in the inertial system of reference, and ii) reach galactocentric distances exceeding 10^2 times the truncation radius of our galaxy model, thus making extremely implausible a recapture. Using this procedure, we identified 362 escaping stars in the galaxy hosting the 5×10^8 M$_\odot$ massive BH, that is 2.4% of the total number of stars of the GC. Scaling this number to the

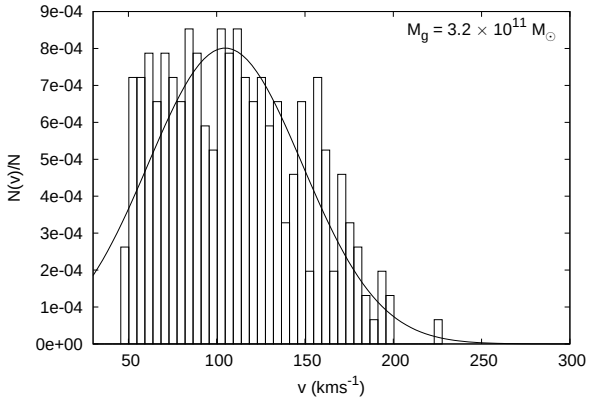

Figure 9. Velocity distribution of escapers 63 Myr after the GC passage at perigalacticon for a cluster containing 10^6 stars. All the stars in the plot have distance from the galaxy centre larger then 1 kpc. The black line indicates a gaussian fit with mean value 103 ± 3 km s^{-1} and dispersion 46.5 ± 3.8 km s^{-1}.

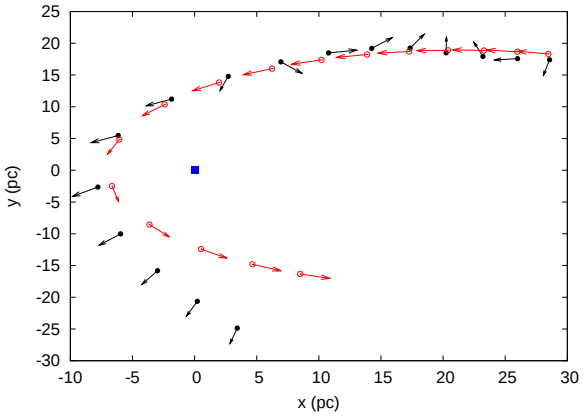

Figure 10. Production of a high-velocity star (black dot) in our simulation. The black vector represents the velocity of the escaping star while the red vector identifies the velocity of the GC centre of density. The blue square is the central SMBH.

total number of stars of a realistic GC, say 10^6 stars, we obtain a population of $\sim 24,000$ stars, formerly belonging to the GC, which wander in the outer region of the galaxy, with velocities in the range $50 - 250$ kms^{-1} and positive total energy. Figure 9 shows the velocity distribution of the whole population of escaping stars.

We found that the escapers have residual velocity up to 250 km s^{-1}, a value comparable to the velocities of high-velocity stars detected in the Milky-Way (Blaauw 1961; Poveda et al. 1967; Hobbs et al. 2005; Brown et al. 2006; Silva & Napiwotzki 2011; Brown et al. 2012, 2014), but definitively smaller than that of the hyper-velocity stars, whose velocities can exceed $800 - 1000$ km s^{-1} (Hills 1988; Yu & Tremaine 2003; Gualandris et al. 2005; Sesana et al. 2006; Sari et al. 2010).

Recently, Brown et al. (2014) have shown that most of the high-velocity stars observed in our galaxy are located in a preferential region, near the galactic North Pole. Of course, this anistropic distribution may hidden some clues related to their origin.

Intriguingly, we notice here that the interaction between an infalling GC and a SMBH seems to represent a significant channel of formation of high-velocity stars, producing a collimated beam of stars that, in a certain fraction, can even escape from the host galaxy. Hence, this channel deserve further investigations (Capuzzo-Dolcetta & Fragione 2015).

Likely, the correct interpretation of the velocity gain is by mean of a 3-body interaction among the GC, the SMBH and the generic star of the cluster. The basic concept, recently developed in Capuzzo-Dolcetta & Fragione (2015), is that some stars of the cluster during its fly-by around the SMBH gain enough kinetic energy, subtracted to the GC-SMBH pair, to be expelled from the GC and even from the galaxy.

Figure 10 shows the velocity vector of one of the escaping stars in simulation $M_g = 3.2 \times 10^{11}$ M$_\odot$, as it moves around its GC, which, in its turn, is moving around the SMBH. After the passage at pericentre, it is evident that the star, which is behind the GC with respect to the GC-SMBH direction, is accelerated and thrown away along the direction tangential to the GC orbit.

This 3-body mechanism is similar to the interaction between the SMBH and a binary star proposed by Hills (1988), but in this case the "primary" member of the binary is the whole GC, or at least the fraction of the cluster mass enclosed within the trajectory of the "secondary" (the future escaping star). Using the parallelism with the treatment of Hills (1988), later revisited by Yu & Tremaine (2003) and Sari et al. (2010), we can give a rough estimate of the ejection velocities of stars gaining kinetic energy at distance r_* from the GC center, that, in the case of a GC Plummer profile gives

$$v_{\rm ej}({\rm km\ s^{-1}}) = 108 \left(\frac{M_{\rm BH}}{10^6\ {\rm M_\odot}}\right)^{\frac{1}{6}} \left(\frac{M}{10^6\ {\rm M_\odot}}\right)^{\frac{1}{3}} \left(\frac{1\ {\rm pc}}{r_P}\right)^{\frac{1}{2}} \left(\frac{x_*}{1+x_*^2}\right)^{\frac{1}{2}} \quad (8)$$

which maximizes for $x_* = r_*/r_P = 1$, where r_P is the profile scale length. During the passage at pericentre, the GC half-mass radius for our model is $r_h = 0.8 \pm 0.2$. For a Plummer sphere, $r_h \approx 1.3 r_P$; therefore, for our GC model $r_P = 0.6 \pm 0.1$ pc, value very close to the peak of the velocity distribution in one of our N-body simulation (see Fig. 11) which can be considered quite representative of simulations presented in this paper.

6 CONCLUSIONS

In this paper we gave an interpretation of the observed dearth of NSCs in massive host galaxies. The problem was studied by performing several high-precision, direct, N-body simulations of the orbital decay of a massive GC in a galaxy harboring a central SMBH. To run our simulations we employed the `HiGPUs` code (Capuzzo-Dolcetta et al. 2013). These simulations allowed us to quantify the combined role of dynamical friction and of tidal forces on the cluster along its motion.

Our results can be summarized as follows:

- in all the cases studied (different masses for the host galaxy and for the central black hole, different initial orbits

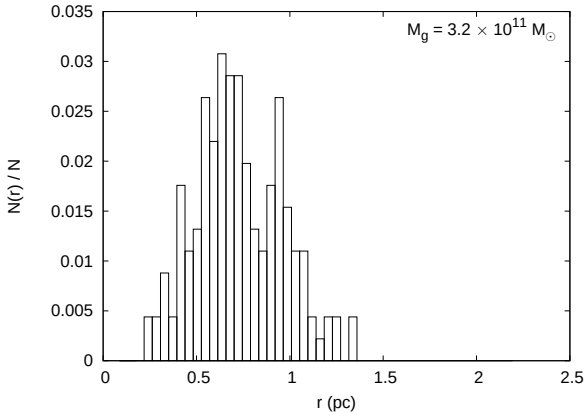

Figure 11. Spatial distribution, with respect to the GC COD, of the escapers that gain the largest kicks during the passage at pericentre. We considered here only stars with velocities greater than the escapers mean velocity, $\simeq 103$ km s^{-1}. The distribution, fitted with a gaussian distribution, peaks at $r = 0.71 \pm 0.24$ pc.

for the "test" GC, as summarized in Table 1), we found that the main contribution to the "tidal heating" of the cluster was given by the central SMBH, accompanied by a less relevant and slower erosion caused by the stellar galactic background;

- in galaxies below 10^{11}M$_\odot$, the cluster transports to the galactic centre more than 80% of its initial mass, regardless of the shape of the initial orbit. On the other side, in heavier galaxies we showed that the mass deposited to the central galactic region by the cluster on the nearly radial orbit is limited to 20% of its initial mass, while the cluster moving on the initially circular orbit is almost completely disrupted after its first crossing of the galactic centre, thus giving a negligible contribution to the formation of a bright nucleus therein;
- by means of scaling arguments we showed that in galaxies more massive than 10^{11}M$_\odot$ the formation of a clearly detectable stellar projected overdensity (a NSC) should occur only when the total mass of the decayed clusters (of the size and with the characteristics studied in this paper) is $\sim 10^8$M$_\odot$, an order of magnitude above the value expected from observational and theoretical arguments.
- in the case of GC eccentric and radial orbits we found that, as the cluster passes through the perigalacticon in the case $M_g = 3.2 \times 10^{11}$M$_\odot$, a small quantity of the cluster stars is "thrown" away from the galactic centre reaching distances above 5 kpc with residual velocities up to 250 kms^{-1}. A fraction of these stars reach velocities such to become unbound from the galaxy. Rescaling these results to a real globular cluster, with $\sim 10^6$ stars, this corresponds to more than 10^4 escapers. The anisotropy in the escapers distribution and the velocities that they gained suggest that this sort of 3-body mechanism (GC+SMBH+star orbiting the GC) is a valid mode of formation of high-velocity stars. This deduction finds a nice confirmation in that the velocity distribution of the escapings stars in our N-body simulations peaks for stars receiving the kick when they transit at a distance from the GC center equal to the Plummer length scale of the analytical model on which we based our 3-body considerations, following the original Hills (1988) approach.

AKNOWLEDGEMENTS

The authors warmly thank S. Mikkola for providing his code implementing the algorithmic regularization, and for his useful comments and suggestions about the star-ejection mechanism discussed in this paper.

MAS acknowledges the MIUR, which funded part of this research through the grant PRIN PRIN 2010 LY5N2T 005, and the financial support from the University of Rome Sapienza through the grant D.D. 52/2015 in the framework of the research programme "The MEGaN project: Modelling the Evolution of GAlactic Nuclei".

MS acknowledges financial support from the Italian Ministry of Education, University and Research (MIUR) through grant FIRB 2012 RBFR12PM1F.

REFERENCES

Antonini F., 2013, ApJ, 763, 62
Antonini F., Barausse E., Silk J., 2015a, ApJ, 812, 72
Antonini F., Barausse E., Silk J., 2015b, ApJL, 806, L8
Antonini F., Capuzzo-Dolcetta R., Mastrobuono-Battisti A., Merritt D., 2012, ApJ, 750, 111
Arca-Sedda M., Capuzzo-Dolcetta R., 2014a, ApJ, 785, 51
Arca-Sedda M., Capuzzo-Dolcetta R., 2014b, MNRAS, 444, 3738
Arca-Sedda M., Capuzzo-Dolcetta R., Antonini F., Seth A., 2015, ApJ, 806, 220
Bekki K., 2007, PASA, 24, 77
Bekki K., Graham A. W., 2010, ApJL, 714, L313
Binney J., Tremaine S., 2008, Galactic Dynamics: Second Edition. Princeton University Press
Blaauw A., 1961, Bull. Astron. Inst. Netherlands, 15, 265
Böker T., Laine S., van der Marel R. P., Sarzi M., Rix H.-W., Ho L. C., Shields J. C., 2002a, AJ, 123, 1389
Böker T., Laine S., van der Marel R. P., Sarzi M., Rix H.-W., Ho L. C., Shields J. C., 2002b, AJ, 123, 1389
Böker T., Sarzi M., McLaughlin D. E., van der Marel R. P., Rix H.-W., Ho L. C., Shields J. C., 2004, AJ, 127, 105
Brown W. R., Cohen J. G., Geller M. J., Kenyon S. J., 2012, ApJL, 754, L2
Brown W. R., Geller M. J., Kenyon S. J., 2014, ApJ, 787, 89
Brown W. R., Geller M. J., Kenyon S. J., Kurtz M. J., 2006, ApJL, 640, L35
Capuzzo-Dolcetta R., 1993, ApJ, 415, 616
Capuzzo-Dolcetta R., Fragione G., 2015, ArXiv e-prints
Capuzzo-Dolcetta R., Miocchi P., 2008a, ApJ, 681, 1136
Capuzzo-Dolcetta R., Miocchi P., 2008b, MNRAS, 388, L69
Capuzzo-Dolcetta R., Spera M., Punzo D., 2013, Journal of Computational Physics, 236, 580
Carollo C. M., Danziger I. J., Rich R. M., Chen X., 1997, ApJ, 491, 545
Côté P., Blakeslee J. P., Ferrarese L., Jordán A., Mei S., Merritt D., Milosavljević M., Peng E. W., Tonry J. L., West M. J., 2004, ApJS, 153, 223
Côté P., Piatek S., Ferrarese L., Jordán A., Merritt D., Peng E. W., Haşegan M., Blakeslee J. P., Mei S., West M. J., Milosavljević M., Tonry J. L., 2006, ApJS, 165, 57
Dehnen W., 1993, MNRAS, 265, 250
den Brok M., Peletier R. F., Seth A., Balcells M., Dominguez L., Graham A. W., Carter D., Erwin P., Ferguson H. C., et al . 2014, MNRAS, 445, 2385
Emsellem E., 2013, MNRAS, 433, 1862
Erwin P., Gadotti D. A., 2012, Advances in Astronomy, 2012

Ferrarese L., Côté P., Dalla Bontà E., Peng E. W., Merritt D., Jordán A., Blakeslee J. P., Haşegan M., Mei S., Piatek S., Tonry J. L., West M. J., 2006, ApJL, 644, L21
Ferrarese L., Ford H., 2005, Space Sci. Rev. , 116, 523
Geha M., Guhathakurta P., van der Marel R. P., 2002, AJ, 124, 3073
Graham A. W., 2012, MNRAS, 422, 1586
Graham A. W., 2015, ArXiv e-prints
Graham A. W., Driver S. P., 2007, ApJ, 655, 77
Graham A. W., Onken C. A., Athanassoula E., Combes F., 2011, MNRAS, 412, 2211
Graham A. W., Spitler L. R., 2009, MNRAS, 397, 2148
Gualandris A., Portegies Zwart S., Sipior M. S., 2005, MNRAS, 363, 223
Hernquist L., 1990, ApJ, 356, 359
Hills J. G., 1988, Nature, 331, 687
Hobbs G., Lorimer D. R., Lyne A. G., Kramer M., 2005, MNRAS, 360, 974
Hopkins P. F., Quataert E., 2010, MNRAS, 407, 1529
King A., 2003, ApJL, 596, L27
King A., 2005, ApJL, 635, L121
King I. R., 1966, AJ, 71, 64
Kormendy J., Ho L. C., 2013, ARA& A, 51, 511
Leigh N., Böker T., Knigge C., 2012, MNRAS, 424, 2130
McLaughlin D. E., King A. R., Nayakshin S., 2006, ApJL, 650, L37
McMillan P. J., Dehnen W., 2007, MNRAS, 378, 541
Mei S., Blakeslee J. P., Côté P., Tonry J. L., West M. J., Ferrarese L., Jordán A., Peng E. W., Anthony A., Merritt D., 2007, ApJ, 655, 144
Merritt D., 2006, Reports on Progress in Physics, 69, 2513
Merritt D., 2013, Dynamics and Evolution of Galactic Nuclei
Mikkola S., Tanikawa K., 1999, MNRAS, 310, 745
Milosavljević M., 2004, ApJL, 605, L13
Nayakshin S., Wilkinson M. I., King A., 2009, MNRAS, 398, L54
Neumayer N., 2012, ArXiv e-prints
Neumayer N., Walcher C. J., Andersen D., Sánchez S. F., Böker T., Rix H.-W., 2011, MNRAS, 413, 1875
Plummer H. C., 1911, MNRAS, 71, 460
Poveda A., Ruiz J., Allen C., 1967, Boletin de los Observatorios Tonantzintla y Tacubaya, 4, 86
Preto M., Tremaine S., 1999, AJ, 118, 2532
Richstone D., Ajhar E. A., Bender R., Bower G., Dressler A., Faber S. M., Filippenko A. V., Gebhardt K., Green R., Ho L. C., Kormendy J., Lauer T. R., Magorrian J., Tremaine S., 1998, Nature, 395, A14
Rossa J., van der Marel R. P., Böker T., Gerssen J., Ho L. C., Rix H.-W., Shields J. C., Walcher C.-J., 2006, AJ, 132, 1074
Sari R., Kobayashi S., Rossi E. M., 2010, ApJ, 708, 605
Scott N., Graham A. W., 2013, ApJ, 763, 76
Sesana A., Haardt F., Madau P., 2006, ApJ, 651, 392
Shankar F., Weinberg D. H., Miralda-Escudé J., 2009, ApJ, 690, 20
Silva M. D. V., Napiwotzki R., 2011, MNRAS, 411, 2596
Tremaine S. D., 1976, ApJ, 203, 345
Tremaine S. D., Ostriker J. P., Spitzer Jr. L., 1975, ApJ, 196, 407
Turner M. L., Côté P., Ferrarese L., Jordán A., Blakeslee J. P., Mei S., Peng E. W., West M. J., 2012, ApJS, 203, 5
Urry C. M., Padovani P., 1995, PASP, 107, 803
van den Bosch R. C. E., Gebhardt K., Gültekin K., van de Ven G., van der Wel A., Walsh J. L., 2012, Nature, 491, 729
Walcher C. J., van der Marel R. P., McLaughlin D., Rix H.-W., Böker T., Häring N., Ho L. C., Sarzi M., Shields J. C., 2005, ApJ, 618, 237
Wehner E. H., Harris W. E., 2006, ApJL, 644, L17
Yu Q., Tremaine S., 2003, ApJ, 599, 1129